

Direct Visual Evidence for Quinoidal Charge Delocalization in Poly-*p*-phenylene Cation Radical

Mengtao Sun,^{*,†} Yong Ding,^{‡,§} and Hongxing Xu^{†,||}

Beijing National Laboratory for Condensed Matter Physics, Institute of Physics, Chinese Academy of Sciences, P.O. Box 603-146, Beijing, 100080, P. R. China, Department of Physics, Liaoning University, Shenyang, 110036, China, Department of Physics, Peking University, Beijing, 100871, P. R. China, and Division of Solid State Physics, Lund University, Lund 22100, Sweden

Received: August 14, 2007; In Final Form: September 11, 2007

Recently, X-ray crystallographic evidence of quinoidal charge delocalization in poly-*p*-phenylene cation radicals was reported [Banerjee, M. et al., *J. Am. Chem. Soc.* **2007**, *129*, 8070]. In this paper, direct visual evidence for quinoidal charge delocalization in quaterphenylene (QP) is shown with three-dimensional (3D) charge difference densities. It was revealed that the extra positive charge mainly localized on the two center units at the ground state, while the extra positive charge will delocalize to the two outer units upon electronic state transitions by photoexcitation. The 2D plots together with the corresponding charge difference densities were interpreted as large distance–charge oscillations, implying that in the positive species upon excitation a nearly free oscillating motion of a hole occurs. For the QP cation radical, the transition dipole moment of S_1 represents mesoscopic dipole antennae.

Introduction

The optoelectronic properties of conjugated polymers are of interest because of their unique optical and electronic properties as semiconductors and possible applications to light-emitting diodes, photovoltaic devices, field-effect transistors, biosensors, imaging devices, and solid-state lasers.^{1–5} Poly-*p*-phenylenes (PPPs), as the simplest aromatic polymers, are potentially one of the most useful classes of polymers for organic conducting materials and organic polymeric ferromagnets because of their extended planar conjugated π system, along with strength, high heat resistance, and oxidative stability.^{6,7} It is well-known that PPP becomes a highly conducting n- or p-type material when it complexes respectively with either reductants (Na, K, or Li) or oxidants (AsF₅, SbF₅, BF₃, or PF₆).⁸ The theoretical research on conducting polymers has been mainly concerned with radical and ionic sites, referred to as the neutral radical and charged defects, respectively.

To study the influence of extra positive charge (cation radical) on the structure of neutral poly-*p*-phenylenes (PPP), and to study the charge redistribution of the PPP cation radical in the electronic state transitions by photoexcitation, the oxidized polyphenyl cation radical has been isolated, and the X-ray crystallographic evidence of quinoidal charge delocalization in PPP cation radicals was reported recently.⁹

In this paper, the electronic structure and charge transfer of PPP cation radicals were studied theoretically. We first describe the distribution of the extra positive charge at the ground state; then we present the direct visual evidence for quinoidal charge delocalization in quaterphenylene (QP) in electronic state transitions by photoexcitation with charge difference density (CDD).^{10–13} To study the electron–hole coherence in the charge

transfer, exciton and oscillation of electron–hole pairs were investigated with 2D site representation.^{12–14} The different capabilities of charge transfer in different electronic state transitions was interpreted with transition density measurement.¹⁵

Methods

All of the calculations reported in this paper were carried out using the Gaussian suite of programs.¹⁶ The *tert*-butyl groups at the terminal positions of QP (see the insert in Figure 1) in the experiment were replaced by H in our calculations, because they merely aid in improving solubility without affecting electronic properties.¹⁷ The ground-state geometry of the QP cation radical was optimized with density functional theory (DFT),¹⁸ using B3LYP functional^{19–21} and 6-31G(D) basis set. Vibrational frequency calculations at the same level of theory were carried out, and there is no imaginary part (see Figure A and Table A in Supporting Information), which confirms that it was the minimum energy structure in the potential energy landscape. The optimized minimum energy structure was used for time-dependent DFT (TD-DFT)²² calculations using the same functional and basis set to the optical absorption properties. In our calculations the expected value of the total spin $\langle S^2 \rangle = s(s + 1)$ for the cation radical QP is 0.7608 before and 0.7501 after annihilation of the first spin contaminant, indicating that the spin contamination is negligible. To check the effect of the basis set on the optical absorption properties, TD-B3LYP/6-311++G-(2d,p)/DFT-B3-LYP/6-311++G(2d,p) were used to reproduce the absorption spectrum.

To examine the influence of the solvent (dichloromethane in the experiment in ref 9) on the absorption spectrum, the ground-state geometry was calculated with the level of DFT-B3-LYP/6-31G(D) and with the Polarizable Continuum Model (PCM),²³ where the value of the dielectric constant is $\epsilon = 8.93$. Vibrational frequency calculations at the same level of theory were carried out, and there is no imaginary part (see Figure B and Table B

* Corresponding author. Email: mtsun@aphy.iphy.ac.cn.

† Chinese Academy of Sciences.

‡ Peking University.

§ Liaoning University.

|| Lund University.

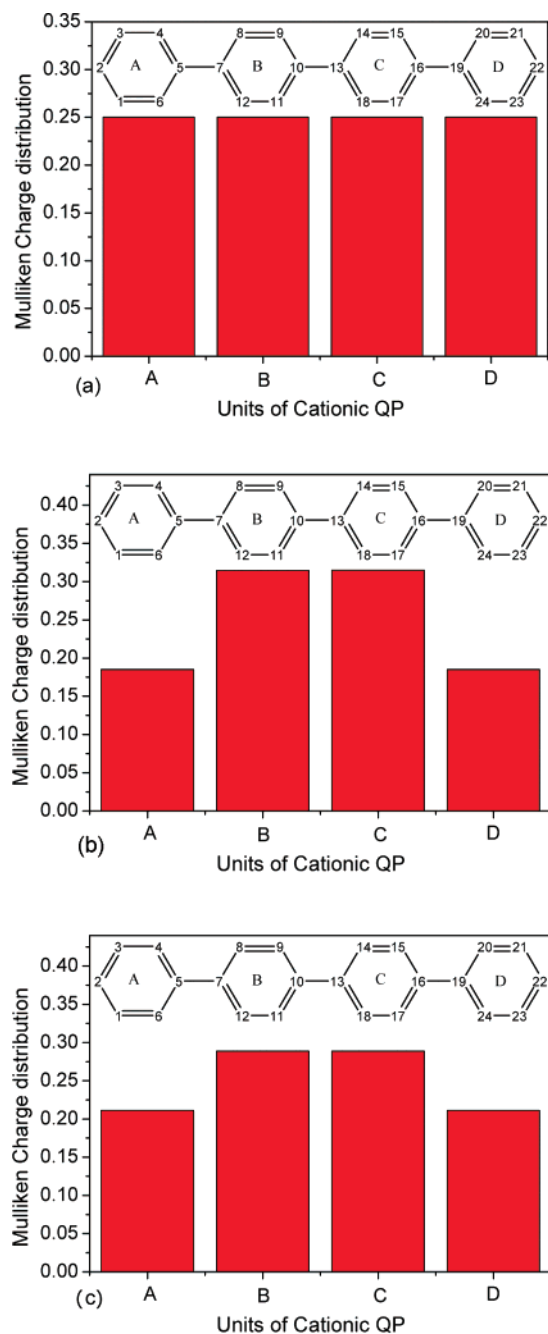


Figure 1. The distribution of Mulliken charges on the four units in the gas phase, which were calculated (a) with DFT-B3LYP/6-31G(D), and (b) with DFT-B3-LYP/6-311++G(2d,p), and (c) the distribution of Mulliken charges on the four units in solvent of dichloromethane, which were calculated with DFT-B3LYP/6-31G(D) and PCM model. The chemical structure of QP was inserted, where the numberings of atoms were used in Figure 3. A, B, C, and D stand for four different units in the abscissa, while in the y-coordinate, the numbers stand for the positive charges on the atoms in these units.

in Supporting Information), which confirms that it was the minimum energy structure in the potential energy landscape. The optimized minimum energy structure was used for TD-DFT calculations using the same functional and basis set and PCM for the absorption properties. In our calculations with the solvent, the expected value of the total spin $\langle S^2 \rangle = s(s + 1)$ for the QP cation radical is 0.7608 before and 0.7501 after annihilation of the first spin contaminant, indicating that the spin contamination is negligible.

The charge transfer in the QP cation radical in the electronic state transitions was investigated with charge difference density.

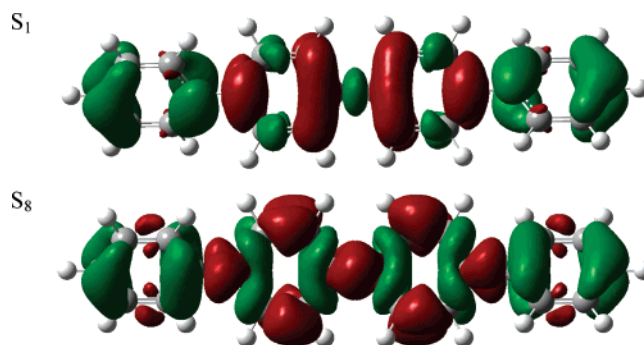


Figure 2. The charge difference densities of S_1 and S_8 , where the green and red stand for the hole and electron, respectively.

The electron–hole coherence on the charge transfer was investigated with 2D site representation. The orientation and strength of the transition dipole moment of the QP cation radical were revealed with transition density measurement.

Results and Discussion

1. Ground State Properties of the QP Cation Radical.

From the optimized ground-state properties in the gas phase, the Mulliken charges calculated with the level of DFT-B3LYP/6-31G(D) almost equally distribute on the four units (see Figure 1(a)), while considering the diffuse functional, the Mulliken charges on the two central units are much larger than those on the two outer units, and the ratio of extra positive charges on the two outer units over all the extra positive charges is 37% (see Figure 1(b), calculated with the level of DFT-B3-LYP/6-311++G(2d,p)). So, the calculated distribution of Mulliken charges in the ground state in the gas phase was affected by the choice of the diffuse functional. With the diffuse functional, the Mulliken charges on the two central units are larger than those on the two outer units. Considering the solvent effect (the interaction energy of the polarized solute–solvent is -37.29 kcal/mol), the Mulliken charge distribution (see Figure 1(c)) on the four units is similar to that of the results calculated with DFT-B3-LYP/6-311++G(2d,p) in the gas phase. Comparing them with the experimental result in ref 9, the distribution of Mulliken charges in Figures 1(b) and 1(c) are consistent with the experimental data (the charges on the two inner units are larger than those on the two outer units in the experiment in ref 9). The difference between the calculated extra positive charge and the experimental results in the X-ray work in ref 9 is that the experimental asymmetric charge distribution attests to the strong electronic coupling within the “shifted” dimeric associates,⁹ which was not considered in the theoretical calculation.

2. Optical Absorption Spectrum of the QP Cation Radical.

The experimental twin absorption bands at $\lambda_{\max} = 490$ and 1302 nm were reproduced with TD-DFT. The calculated transition energies and oscillator strengths of the QP cation radical are listed in Table 1. It is confirmed that the influence of the basis set on the absorption spectrum in the gas phase is small for this system. From the data in Table 1, the solvent effect causes an absorption spectrum red-shift of about 50 nm for the first peak, comparing the calculated electronic state transition energies in the gas phase, while for the shift of the second peak in the absorption spectrum, the solvent effect is small. To check the effect of the substitutions at the terminal positions on the electronic state absorption, the *tert*-butyl groups of QP at the terminal positions in the experiment were also replaced by CH_3 , and the electronic state transitions were calculated with TD-B3LYP/6-31G(D)/DFT-B3-LYP/6-31G(D) in the gas phase. It

TABLE 1: The Experimental and Theoretical Transition Energies (nm) and Oscillator Strength (*f*)

	exptl ^a	calcd (solvent) ^b		calcd (gas phase) ^c		calcd (gas phase) ^d		calcd (gas phase) ^e	
	Nm	nm	<i>f</i>	nm	<i>f</i>	nm	<i>f</i>	nm	<i>f</i>
S ₁	1302	1064.49	0.7525	1013.82	0.6090	1010.41	0.6116	1094.67	0.6730
		848.09	0.0003	933.07	0.0002	904.26	0.0002	854.90	0.0004
		843.31	0.0003	931.36	0.0002	902.17	0.0002	852.97	0.0002
		778.47	0.0004	747.03	0.0001	736.02	0.0001	716.91	0.0001
		733.04	0.0001	706.65	0.0000	691.54	0.0000	677.78	0.0000
		629.67	0.0000	635.78	0.0000	631.44	0.0000	664.34	0.0000
		446.39	0.0944	448.25	0.0341	445.98	0.0684	451.05	0.0869
S ₈	490	421.67	0.8842	413.02	0.8699	418.57	0.8502	426.58	0.9132

^a Experimental result from ref 9. ^b Calculated result with TD-B3LYP/6-31G(D)//DFT-B3LYP/6-31G(D) and PCM model, where the dielectric constant is 8.93. ^c Calculated result with TD-B3LYP/6-31G(D)//DFT-B3-LYP/6-31G(D) in the gas phase. ^d Calculated result with TD-B3LYP/6-311++G(2d,p)//DFT-B3-LYP/6-311++G(2d,p) in the gas phase. ^e Calculated result with TD-B3LYP/6-31G(D)//DFT-B3-LYP/6-31G(D) in the gas phase, where the H substituents of QP were replaced by CH₃.

TABLE 2: Ground to Excited State Transition Electric Dipole Moments (au and Debye) Calculated with TD-B3LYP/6-31G(D) and PCM

	X		Y		Z	
	au	Debye	au	Debye	au	Debye
S ₁	5.1352	13.0434	0.0000	0.0000	0.0000	0.0000
S ₈	3.5034	8.8986	0.0000	0.0000	0.0000	0.0000

can be found from Table 1 that the CH₃ substitutions at the terminal positions have little influence on the shift in the absorption spectrum.

The difference between the experimental and theoretical results in the optical absorption spectra is from the possible impact of nuclear vibration. According to the report by Banerjee et al., the structure of QP is warped.⁹ They insist that there is charge delocalization in this kind of structure. Therefore, when it is applied to artificial systems, it is expected that static or dynamic effects from the nuclear vibration would cause fluctuation in the electronic states. Another reason is that strong electronic coupling⁹ between QP⁺ systems was not considered in the calculation.

3. Excited-State Properties of Cation Radical QP in Absorption. According to above analysis about the Mulliken charge distribution on the four units and the calculated absorption spectrum, the calculation with the level of TD-DFT/B3LYP-6-31G(D) and PCM can best reproduce the ground state properties and absorption spectrum of QP in the experiment in ref 9. So, the excited-state properties we studied below were based on the results calculated with the level of TD-DFT/B3LYP-6-31G(D) and PCM. The orbital transitions for electronic state transitions (the two peaks) in the absorption spectrum are listed in Table C in the Supporting Information. In the analysis of the excited-state properties of the QP cation radical in optical absorption, only the strongest CI coefficients were considered for simplification.

The excited properties of twin absorption peaks of the QP cation radical were revealed with charge difference densities, which allow us to follow the change of the static charge distribution upon excitation. From the charge difference densities of S₁ and S₈ in Figure 2, most extra positive charges move to two outer units upon excitation, which were mostly localized on the two central units at ground state (see Figure 1(c)). So, by comparing the charge distributions at ground state (Figure 1(c)) and those at the excited states (Figure 2), direct visual evidence for quinoidal charge delocalization in the PPP cation radical can be clearly derived. It should be noted that “the distribution of electron and hole” really refers to the difference of their distributions between the ground and excited states. Comparing the charge distribution at S₁ and that at S₈, one can

find that the most difference is between the distributions of hole and electron at the two central units. For example, for S₁, the holes reside on the single bond which links two central phenyls, while for S₈, the electrons reside on single bonds which link phenyls. Furthermore, the distribution of electron and hole on the two central units are significantly different.

To study the detailed differences of charge distribution on S₁ and S₈, the electron–hole coherences for these two excited states were investigated with 2D site representation. The contour plots of transition density matrixes can be seen in Figure 3, where $|Q|^2$ is a measure of the delocalization of the exciton as a whole, while $|P|^2$ describes the oscillation of electron and hole from the atomic sites a and b.¹² Clearly the exciton for S₁ is within two adjacent units (AB units and CD units, see $|Q|^2$), while the oscillation of electron–hole is between AB units and CD units, which reveals that S₁ is a strong charge transfer (between AB and CD) excited state (see $|P|^2$). The plots together with the corresponding charge difference densities were interpreted as large distance–charge oscillations, implying that in the positive species upon excitation a nearly free oscillating motion of a hole occurs. In this way, the lowest electronic transition of the cationic species can be seen as an “intra-band” excitation; electrons are excited inside the conduction band and the corresponding holes in the valence band.²⁴

Comparing $|Q|^2$ of S₁ and that of S₈, a conclusion can be derived that the exciton of S₈ is not strongly localized within two adjacent units ((AB units and CD units) but rather is much delocalized. Comparing $|P|^2$ of S₁ and that of S₈, the ability of charge transfer between units of S₈ is much weaker than that of S₁, which can also be confirmed by charge difference densities in Figure 2. From the charge difference densities, all the electrons transferred to the two central units for S₁, while there are still electrons on the single bonds that link the outer and central units. Furthermore, there are still some electrons on the outer units.

The transition dipole moment of S₁ (along the molecular axis) is stronger than that of S₈, which can be seen in Table 2. The transition density indicates that the transition dipole moment for S₁ is much stronger than that of S₈, since the transition density $\rho_{\lambda 0}$ contains information about the spatial location of the excitation and is directly related to the transition dipole¹⁰

$$\mu_{\lambda 0} = e \int r \rho_{\lambda 0}(r) d^3 r \quad (1)$$

From transition densities in Figure 4, the real space transition densities for S₁ show significantly different characteristic features from that of S₈. While the transition density for S₈ alternates in sign on the conjugated chain, that of S₁ is divided into two regions with constant sign and a node in the central

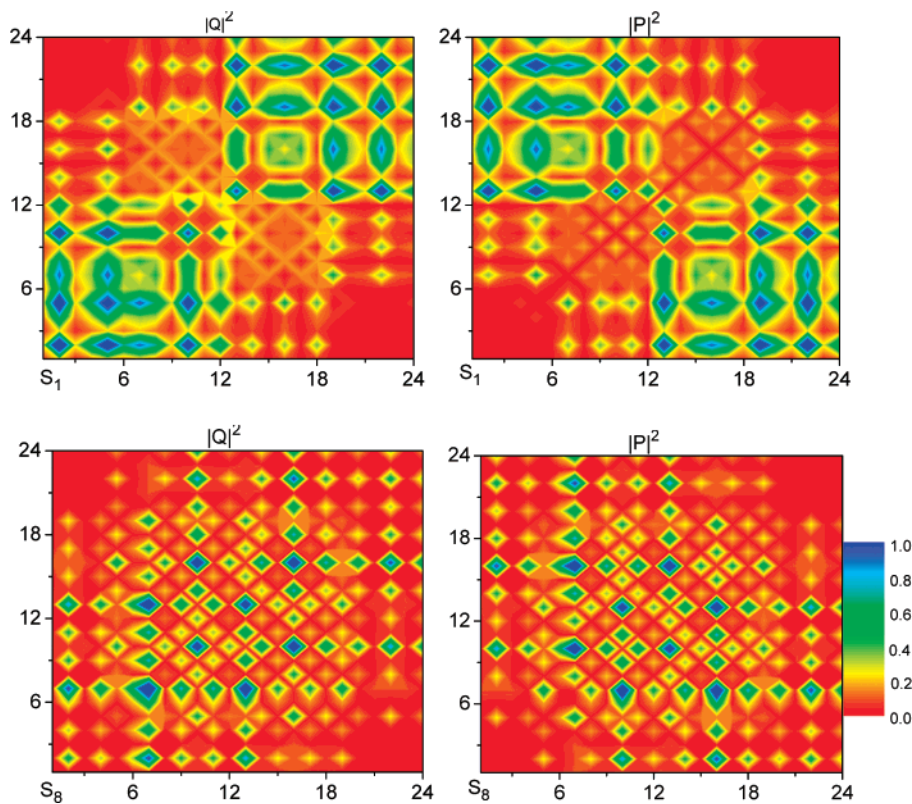


Figure 3. The contour plots of 2D site representation (transition density matrix). The color bar is shown at the right of the last picture. Numbering of atoms can be seen from the insert in Figure 1.

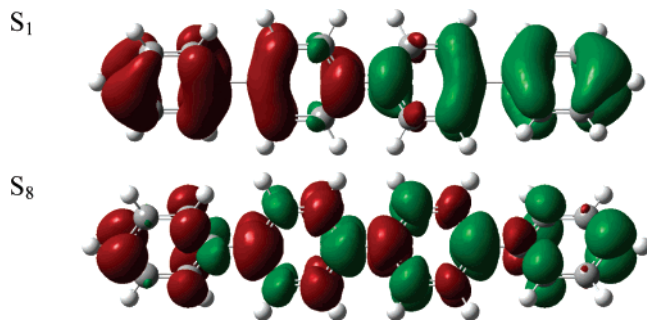


Figure 4. The transition densities of S_1 and S_8 , where the green and red stand for the hole and electron, respectively.

ring. Thus, the transition dipole moment of S_1 represents mesoscopic dipole antennae, while the transition dipole moment of S_8 should rather be represented by a series of small transition dipoles, one per monomeric unit.¹² It should be noted that the dipole moment calculated with eq 1 is the dynamic transition dipole moment on the electronic state transition ($\mu_{\lambda,0}$), not the permanent static dipole moments at the ground and excited states ($\mu_{0,0}$ and $\mu_{\lambda,\lambda}$). The $\mu_{0,0}$ and $\mu_{\lambda,\lambda}$ values should be quite small, since the structure of QP is centrosymmetric.

Conclusion

The distribution of charge on the ground and excited states were investigated with charge difference density, which shows direct visual evidence for quinoidal charge delocalization in the PPP cation radical. The 2D site plots together with the corresponding charge difference densities were interpreted as large distance–charge oscillations, implying that in the positive species upon excitation a nearly free oscillating motion of a hole occurs. The transition dipole moment of S_1 represents mesoscopic dipole antennae.

Acknowledgment. This work was supported by the National Natural Science Foundation of China (Grant Nos.10505001, 10625418, and 20703064), the National Basic Research Project of China (Grant Nos. 2007CB936801 and 2007CB936804), the Sino-Swedish collaborations about nanophotonics and nano-electronics (2006DFB02020), and the “Bairen” projects of CAS.

Supporting Information Available: Calculated IR absorption spectrum and vibrational frequencies with DFT-B3LYP/6-31G(D) in the gas phase; calculated IR absorption spectrum and vibrational frequencies with DFT-B3LYP/6-31G(D) and PCM model; CI coefficients calculated with TD-B3LYP/6-31G(D)//DFT-B3-LYP/6-31G(D) and PCM. This material is available free of charge via the Internet at <http://pubs.acs.org>.

References and Notes

- (1) Burroughes, J. H.; Bradley, D. D. C.; Brown, A. R.; Marks, R. N.; Mackay, K.; Friend, R. H.; Burns, P. L.; Holmes, A. B. *Nature* **1990**, *347*, 539.
- (2) Wang, D. L.; Gong, X.; Heeger, P. S.; Rininsland, F.; Bazan, G. C.; Heeger, A. J. *Proc. Natl. Acad. Sci. U.S.A.* **2002**, *99*, 49.
- (3) Siringhaus, H.; Kawase, T.; Friend, R. H.; Shimoda, T.; Inbasekaran, M.; Wu, W.; Woo, E. P. *Science* **2000**, *290*, 2123.
- (4) Chua, L. L.; Zausmell, J.; Chang, J. F.; Ou, E. C. W.; Ho, P. K. H.; Siringhaus, H.; Friend, R. H. *Nature* **2005**, *434*, 194.
- (5) Chen, M. X.; Crispin, X.; Perzon, E.; Andersson, M. R.; Pullerits, T.; Andersson, M.; Inganäs, O.; Berggren, M. *Appl. Phys. Lett.* **2005**, *87*, 252105.
- (6) Hide, F.; DiazGarcia, M. A.; Schwartz, B. J.; Heeger, A. J. *Acc. Chem. Res.* **1997**, *30*, 430.
- (7) Gale, D. M. *J. Appl. Polym. Sci.* **1978**, *22*, 1971.
- (8) Ivory, D. M.; Miller, G. G.; Sowa, J. M.; Shacklette, L. W.; Chance, R. R.; Baughman, R. H. *J. Chem. Phys.* **1979**, *71*, 1506.
- (9) Banerjee, M.; Lindeman, S. V.; Rathore, R. *J. Am. Chem. Soc.* **2007**, *129*, 8070.
- (10) Jespersen, K. G.; Beenken, W. J. D.; Zausjitsyn, Y.; Yartsev, A.; Andersson, M.; Pullerits, T.; Sundström, V. *J. Chem. Phys.* **2004**, *121*, 12613.
- (11) Beenken, W. J. D.; Pullerits, T. *J. Phys. Chem. B* **2004**, *108*, 6164.

- (12) Sun, M. T.; Kjellberg, P.; Beenken, W. J. D.; Pullerits, T. *Chem. Phys.* **2006**, *327*, 474.
- (13) Sun, M. T.; Liu, L. W.; Ding, Y.; Xu, H. X. *J. Chem. Phys.* **2007**, *127*, 084706.
- (14) Mukamel, S.; Tretiak, S.; Wagersreiter, T.; Chernyak, V. *Science* **1997**, *277*, 781.
- (15) Krueger, B. P.; Scholes, G. D.; Fleming, G. R. *J. Phys. Chem. B* **1998**, *102*, 5378.
- (16) Frisch, M. J.; Trucks, G. W.; Schlegel, H. B.; Scuseria, G. E.; Robb, M. A.; Cheeseman, J. R.; Montgomery, J. A., Jr.; Vreven, T.; Kudin, K. N.; Burant, J. C.; Millam, J. M.; Iyengar, S. S.; Tomasi, J.; Barone, V.; Mennucci, B.; Cossi, M.; Scalmani, G.; Rega, N.; Petersson, G. A.; Nakatsuji, H.; Hada, M.; Ehara, M.; Toyota, K.; Fukuda, R.; Hasegawa, J.; Ishida, M.; Nakajima, T.; Honda, Y.; Kitao, O.; Nakai, H.; Klene, M.; Li, X.; Knox, J. E.; Hratchian, H. P.; Cross, J. B.; Adamo, C.; Jaramillo, J.; Gomperts, R.; Stratmann, R. E.; Yazyev, O.; Austin, A. J.; Cammi, R.; Pomelli, C.; Ochterski, J. W.; Ayala, P. Y.; Morokuma, K.; Voth, G. A.; Salvador, P.; Dannenberg, J. J.; Zakrzewski, V. G.; Dapprich, S.; Daniels, A. D.; Strain, M. C.; Farkas, O.; Malick, D. K.; Rabuck, A. D.; Raghavachari, K.; Foresman, J. B.; Ortiz, J. V.; Cui, Q.; Baboul, A. G.; Clifford, S.; Cioslowski, J.; Stefanov, B. B.; Liu, G.; Liashenko, A.; Piskorz, P.; Komaromi, I.; Martin, R. L.; Fox, D. J.; Keith, T.; Al-Laham, M. A.; Peng, C. Y.; Nanayakkara, A.; Challacombe, M.; Gill, P. M. W.; Johnson, B.; Chen, W.; Wong, M. W.; Gonzalez, C.; Pople, J. A. *Gaussian 03*, revision B.05; Gaussian, Inc.: Pittsburgh, PA, 2003.
- (17) Tolbert, L. M. *Acc. Chem. Res.* **1992**, *25*, 561.
- (18) Dreizler, M. R.; Gross, E. K. U. *Density Functional Theory*; Springer-Verlag: Heidelberg, 1990.
- (19) Becke, A. D. *Phys. Rev. A* **1988**, *38*, 3098.
- (20) Becke, A. D. *J. Chem. Phys.* **1993**, *98*, 5648.
- (21) Lee, C.; Yang, W.; Parr, R. G. *Phys. Rev. B* **1988**, *37*, 785.
- (22) Stratmann, R. E.; Scuseria, G. E.; Frisch, M. J. *J. Chem. Phys.* **1998**, *109*, 8218.
- (23) Cammi, R.; Mennucci, B.; Tomasi, J. *J. Phys. Chem. A* **2000**, *104*, 5631.
- (24) Scheblykin, I. G.; Yartsev, A.; Pullerits, T.; Gulbinas, V.; Sundstrom, V. *J. Phys. Chem. B* **2007**, *111*, 6303.